Ultra-metal-poor Stars: Spectroscopic Determination of Stellar Atmospheric Parameters Using Iron Non-LTE Line Abundances

Rana Ezzeddine, Anna Frebel, Bertrand Plez

Ultra-metal-poor Stars: Spectroscopic Determination of Stellar Atmospheric Parameters Using Iron Non-LTE Line Abundances

Citation: Ezzeddine, Rana et al. "Ultra-Metal-Poor Stars: Spectroscopic Determination of Stellar Atmospheric Parameters Using Iron Non-LTE Line Abundances." The Astrophysical Journal 847, 2 (October 2017): 142 © 2017 The American Astronomical Society

As Published: http://dx.doi.org/10.3847/1538-4357/AA8875

Publisher: IOP Publishing

Persistent URL: http://hdl.handle.net/1721.1/114959

Version: Final published version: final published article, as it appeared in a journal, conference proceedings, or other formally published context

The Astrophysical Journal, 847:142 (12pp), 2017 October 1 https://doi.org/10.3847/1538-4357/aa8875

Ultra-metal-poor Stars: Spectroscopic Determination of Stellar Atmospheric Parameters Using Iron Non-LTE Line Abundances

Rana Ezzeddine[1,2], Anna Frebel[1,2], and Bertrand Plez[3]
[1] Joint Institute for Nuclear Astrophysics, Center for the Evolution of the Elements, East Lansing, MI 48824, USA
[2] Department of Physics and Kavli Institute for Astrophysics and Space Research, Massachusetts Institute of Technology, Cambridge, MA 02139, USA
[3] Laboratoire Univers et Particules de Montpellier, Université de Montpellier, CNRS, UMR 5299, Montpellier, France
Received 2016 November 28; revised 2017 August 10; accepted 2017 August 22; published 2017 October 3

Abstract

We present new ultra-metal-poor stars parameters with $[Fe/H] < -4.0$ based on line-by-line non-local thermodynamic equilibrium (NLTE) abundances using an up-to-date iron model atom with a new recipe for non-elastic hydrogen collision rates. We study the departures from LTE in their atmospheric parameters and show that they can grow up to ∼1.00 dex in [Fe/H], ∼150 K in $T_{\rm eff}$ and ∼0.5 dex in $\log g$ toward the lowest metallicities. Accurate NLTE atmospheric stellar parameters, in particular [Fe/H] being significantly higher, are the first step to eventually providing full NLTE abundance patterns that can be compared with Population III supernova nucleosynthesis yields to derive properties of the first stars. Overall, this maximizes the potential of these likely second-generation stars to investigate the early universe and how the chemical elements were formed.

Key words: line: formation – stars: abundances – stars: atmospheres – stars: fundamental parameters – stars: Population II

Supporting material: machine-readable table

1. Introduction

Ancient ultra-metal-poor (UMP) stars (with $[Fe/H] < -4.0$, e.g., Beers & Christlieb 2005) are rare relics of the early Universe. They provide unique insights into the first nucleosynthesis events and the first (Population III; Pop III hereafter) stars (Klessen et al. 2012; Bromm 2013), the earliest phases of chemical enrichment (Frebel & Norris 2015), as well as the formation of the first low-mass stars (Frebel et al. 2007; Chiaki et al. 2012; Ji et al. 2015). For example, detailed comparisons of supernova nucleosynthesis yields with stellar abundances have shown that Pop III stars were likely massive (20–60 $M_{\odot}$; Keller et al. 2014; Tominaga et al. 2014; Placco et al. 2015), in agreement with theoretical expectations (Abel et al. 2001; Bromm et al. 2002). As more stars and more detailed yield calculations become available, the nature and shape of the initial mass function (IMF) of Pop III stars can ultimately be reconstructed in that way.

Key ingredients are as accurate and precise as possible stellar abundances of many elements. For example, Placco et al. (2015) investigated how abundance availability and precision affected the results of fitting the abundance patterns with nucleosynthetic yields to derive Pop III stellar masses. They found that the exclusion of nitrogen from the abundance pattern had a significant impact on the final derived Pop III progenitor mass. To obtain high-quality chemical abundances, a necessary prerequisite is accurate and precise stellar atmospheric parameters, i.e., effective temperature $T_{\rm eff}$, surface gravity $\log g$, iron abundance [Fe/H], and microturbulence ξ_t that characterize the star. Stellar parameters can be determined in different ways, but in addition to the metallicity, in most cases as least the microturbulence and/or the surface gravity are determined spectroscopically by demanding no abundance trend with a reduced equivalent width and invoking an ionization equilibrium of neutral and singly ionized iron lines, Fe I and Fe II, respectively. The effective temperature can also be determined spectroscopically by invoking the "excitation balance," i.e., no abundance trend with an excitation potential of Fe I lines.

For most abundance analyses, one-dimensional stellar model atmospheres are used, together with radiative transfer codes assuming local thermodynamic equilibrium (LTE). This method, however, is affected by unaccounted departures from LTE that can introduce significant systematic uncertainties, since line formation and populations of non-dominant species (in this case Fe I) can potentially deviate from the Saha–Boltzmann equilibrium assumed in LTE (e.g., Rutten 2003).

Deviations from LTE have been shown to increase toward lower metallicities and for extended atmospheres (giants and super-giants) (Mashonkina et al. 2011, 2016; Bergemann et al. 2012, 2015; Lind et al. 2012). The decreasing number of electrons donated by metals leads to decreased collision rates. In cool, late-type stars ($4000\,{\rm K} < T_{\rm eff} < 6500\,{\rm K}$), lines arising from minority species are most affected by these deviations. To account for such departures, especially in cool UMP stars, it is necessary to investigate the formation of iron lines in non-local thermodynamic equilibrium (non-LTE, hereafter NLTE). For such an investigation, atomic data and other inputs are required for each element. Previous iron NLTE studies have reported abundance changes (∼0.1 dex) simply due to uncertainties in the input atomic data used in their model atoms (Collet et al. 2005; Mashonkina et al. 2011; Bergemann et al. 2012). Particularly problematic in this context are uncertainties arising from estimating the rate of inelastic collisions with neutral hydrogen atoms. They are usually obtained from the classical Drawin approximation (Drawin 1968, 1969a, 1969b; Lambert 1993) because full quantum calculations are lacking. However, the approximation is known to overestimate the collision rates by several orders of magnitude (Barklem et al. 2010; Lind et al. 2011; Osorio et al. 2015). Several attempts to calibrate these rates were made by applying a global multiplicative fudge factor (denoted $S_{\rm H}$) to all the rates, calibrated against different benchmark stars.

However, unlike what is expected for an intrinsic atomic property, different S_H were obtained by different studies and were found to be star-dependent and model-atom-dependent (e.g., Thévenin & Idiart 1999; Korn et al. 2003; Bergemann et al. 2012; Ezzeddine et al. 2016a; Mashonkina et al. 2016).

To obtain more accurate collision rates, a new semi-empirical recipe was proposed by Ezzeddine et al. (2016b), who developed a quantum fitting method (QFM) to estimate the hydrogen collision rates involved in iron line formation and other elements in the absence of available published quantum rates. Transition-energy-dependent recipes for charge-transfer and excitation rates were introduced to determine more reliable Fe abundances. The QFM has already been successfully applied to line formation calculations in solar-type FGK giants and metal-poor stars, such as the Sun, HD 140283, and Arcturus. In this paper, we apply the QFM and our Fe model atom to 20 known UMP stars with $[Fe/H] \lesssim -4.0$. We use high-resolution spectra available in the literature to spectroscopically determine their stellar parameters using NLTE calculations of available Fe lines. This is the first step toward eventually determining their full NLTE abundance patterns.

The paper is structured as follows. In Section 2, we describe the input data used in the NLTE calculations, the iron model atom, and input atomic line lists and model atmospheres. In Section 3, we introduce the method used. Both our LTE and NLTE iron abundances are presented in Section 4, as well as the light element enhancement effects on the final results. In Section 5, we report the NLTE corrections for the LTE iron line abundances, as well as implications for the stellar parameters of the UMP stars. Finally, conclusions are presented in Section 6.

2. Input Data for NLTE Line Formation Calculations

2.1. Iron Model Atom

The iron model atom used in this work was built from all available energy levels for Fe I and Fe II (846 Fe I and 1027 Fe II levels and the Fe III continuum) from the NIST[4] database, which were then collapsed into superlevels, disregarding fine-structure-splitting for all levels except those of Fe I and Fe II ground levels. The model also includes the predicted high-lying Fe I levels from Peterson & Kurucz (2015) that correspond to UV and IR transitions, and establish important collisional couplings with the ground Fe II level. All levels in the atom are coupled via an extensive line list of radiative bound–bound (extracted from VALD3[5] database) and photoionization transitions (extracted from the NORAD[6] database). A detailed description of the iron model atom can be found in Ezzeddine et al. (2016b).

Additionally, all levels in the atom are coupled via electron and hydrogen collisions. These collisions have been shown to have important effects on the final NLTE abundances (an extensive study showing this for Mg is presented in Osorio et al. 2015). While quantum atomic data for the hydrogen collision cross-sections have been computed for some light atoms (Li, Be, Na, Mg, Al, Si and Ca; Belyaev & Barklem 2003; Yakovleva et al. 2016; Barklem et al. 2010; Belyaev et al. 2012; Belyaev 2013; Belyaev et al. 2014, 2016, respectively), data for larger atoms remain scarce and more difficult to compute.

In UMP stellar atmospheres, the hydrogen-to-electron-density ratios can reach up to $\sim 10^5$ due to the scarcity of free electron donors (i.e., metals). This enhances the role that inelastic hydrogen collision rates can play for an NLTE abundance determination. Recently, it has been shown that the charge-transfer (i.e., ion-pair production[7]) processes can dominate over excitation processes (Osorio et al. 2015; Ezzeddine et al. 2016b; Osorio & Barklem 2016). Cross-section calculations for Li+H (Barklem et al. 2003) and Na+H (Barklem et al. 2010), for example, have shown that the largest cross-sections for excitation are small compared with those for ion-pair production from certain energy states. Ion-pair production cross-section calculations for Fe have not been published yet and were thus excluded in most previous NLTE iron studies for UMP stars.

A new semi-empirical QFM to estimate the hydrogen collision rates, including the ion-pair production process, was developed by Ezzeddine et al. (2016b). This method is based on a general fitting recipe deduced from the quantum collision rates of several elements (Be, Na, Mg, Al, Si, and Ca) and then applied to Fe. Tested on 24 *Gaia* benchmark stars (Jofré et al. 2014; Heiter et al. 2015a) with different stellar parameters, it was shown to improve the Fe I and Fe II ionization balance and decrease the obtained abundance scatter, especially for the more metal-poor stars in the sample. This motivates the present work with UMP stars, which are expected to experience significant NLTE abundance effects.

2.2. Line Lists and Equivalent Widths

For our Fe abundance determination, we use absorption lines and equivalent widths measurements for each UMP star from relevant references in the literature. Details are presented in Section 3.1. Log *gf* values for Fe I and Fe II lines from the *Gaia*-ESO "golden" line list v4 (Heiter et al. 2015b) were used. The line list used for each star can be found in Table 1.

2.3. Model Atmospheres

We employ 1D, plane-parallel MARCS atmospheric models (Gustafsson et al. 1975, 2008; Plez 2008), which were interpolated[8] to the corresponding input stellar parameters for each star listed in Table 2. We use models with a metallicity of -5.0 dex for all stars with $[Fe/H] \leqslant -5.0$. Standard α-element enhancement of $[\alpha/Fe] = 0.4$ was adopted for all UMP stars. Blanketing effects were taken into account by including background line opacity tables (excluding Fe) as a function of [Fe/H] and ξ_t (B. Plez 2017, private communication). Throughout, we adopt a reference solar iron abundance of $\log \epsilon(Fe)_\odot = 7.50$ from Asplund et al. (2009).

3. Method

We use the input data introduced in Section 2 (including the Fe model atom, atomic line lists, and 1D MARCS atmospheric models) to determine Fe I and Fe II line-by-line NLTE abundances. We also report the LTE Fe abundance for each UMP star.

[4] https://www.nist.gov/pml/atomic-spectra-database
[5] http://vald.astro.uu.se/
[6] http://www.astronomy.ohio-state.edu/~csur/NORAD/norad.html

[7] During an atomic collision with hydrogen, i.e., A+H, the valence electron associated with atom A has a certain probability of tunneling into the H atom, resulting in a predominantly ionic charge distribution or an ion-pair production $A^+ + H^-$.
[8] The interpolation routine interpol_modeles.f from Thomas Masseron, available at http://marcs.astro.uu.se/software.php, was used.

Table 1
Atomic Line Lists and Obtained Fe I and Fe II Abundances of the UMP Stars

Star Name	Ion	λ (Å)	χ (eV)	log gf	EW (mÅ)	log ε(X)$_{\rm LTE}$ (dex)	log ε(X)$_{\rm NLTE}$ (dex)
SDSS J2209−0028	Fe I	4045.810	1.48	0.28	36.4	3.50	3.82
	Fe I	4063.590	1.56	0.07	31.7	3.67	3.95
	Fe I	4071.740	1.61	−0.02	28.9	3.72	3.99
	Fe I	4383.549	1.48	0.20	28.8	3.36	3.72
	Fe I	4404.750	1.56	−0.14	17.4	3.46	3.78

(This table is available in its entirety in machine-readable form.)

The NLTE radiative transfer code MULTI2.3 (Carlsson 1986, 1992) was used to compute NLTE line profiles using the Accelerated Lambda Iteration (ALI) approximation method (Scharmer 1981). It computes the level populations by solving the statistical equilibrium and radiative transfer equations simultaneously with no feedback from the element in question back into the atmosphere (i.e., considered as a trace element). For each line, the NLTE equivalent width EW$_{\rm NLTE}$ was computed using a Voigt profile function with a maximum of 80 frequency points. We also compute the LTE equivalent width EW$_{\rm LTE}$ from the departure coefficient of each line i, $b^i = {\rm EW}^i_{\rm NLTE}/{\rm EW}^i_{\rm LTE}$ (Wijbenga & Zwaan 1972). A curve-of-growth (COG) method is then used to determine the line abundances that correspond to the observed EW$_{\rm obs}$. All lines used in the abundance analysis lie on the linear part of the COG (log(EW$_{\rm obs}/\lambda$) < -4.8).

3.1. Stellar Atmospheric Parameters

We determined NLTE spectroscopic atmospheric parameters for the UMP stars using NLTE calculations of the abundances of individual Fe I and Fe II lines and upper limits, following the method outlined in Section 3. To guide our calculations, we made use of the fact that stellar parameters for all stars have previously been determined under the assumption of LTE, either fully spectroscopically ($T_{\rm eff}$, log g, ξ_t, and [Fe/H]) or partially (either $T_{\rm eff}$ or log g, ξ_t, and [Fe/H]). We first computed a small grid of NLTE EW at stellar parameters centered around the LTE (or photometric) stellar parameters from the literature (see Section 4). We then compared the corresponding grid of computed NLTE equivalent widths, EW$_{\rm NLTE}$, with the measured observed ones EW$_{\rm obs.}$. This was done for all stars for which EW$_{\rm obs.}$ of at least 5 iron lines could be measured. A first approximation of the initial stellar parameters for each star (in terms of $T_{\rm eff}$, log g, [Fe/H]) was obtained using nonlinear χ^2 fitting of the computed EW$_{\rm NLTE}$ to the observed EW$_{\rm obs.}$ in a $T_{\rm eff}$–log g–[Fe/H] parameter space. This procedure (using a Levenberg–Marquardt algorithm) takes into account that all stellar parameters depend on each other.

In a second step, the excitation balance of Fe I line abundances as a function of the excitation potential of the lower level, χ, of each line, as well as the ionization equilibrium of Fe I and Fe II abundances (when available), were inspected. In the case of an abundance trend with χ or a mismatch between Fe I and Fe II abundances, stellar parameters were adjusted accordingly. In the process, we derived the microturbulent velocity $\xi_{t,\rm NLTE}$ by removing any Fe I line abundance trend with reduced equivalent widths (log(EW$_{\rm obs}/\lambda$)).

4. Results

To proceed with our analysis, we divided our sample of 20 UMP stars into 3 metallicity subgroups following the classification in Placco et al. (2015) as shown in Table 2: hyper-metal-poor (HMP) stars with [Fe/H] < -5.0, stars with $-5.0 <$ [Fe/H] < -4.5, and stars with $-4.5 <$ [Fe/H] < -4.0. We exclude the carbon-rich star G 77−61 from our UMP sample due to the complexity of its spectrum showing very strong CH, CN, and C2 bands around all iron line regions. Its analysis would require the inclusion of CN and C2 lines in the continuum and line background opacities in the NLTE analysis code, which is beyond the scope of the present work. Below we present a brief description of all stars in each subgroup and our stellar parameters in NLTE. We also discuss differences to LTE stellar parameters. Our final NLTE Fe abundances and associated NLTE corrections are further analyzed in Sections 4 and 5, respectively.

4.1. HMP Stars with [Fe/H] < −5

This group includes five stars, SMSS J0313−6708, HE 1327−2326, HE 0107−5240, SDSS J1035+0641, and SDSS J1313−0019, with the lowest iron abundance of [Fe/H] < -5.0, as determined from their LTE analyses.

SMSS J0313−6708 is a warm red giant with the lowest known iron abundance (Keller et al. 2014). Only an upper limit of the Fe abundance could be derived because no Fe lines were detected in the spectrum. The authors determined $T_{\rm eff} = 5125 \pm 100$ K and log $g = 2.3 \pm 0.2$ from spectrophotometry, consistent with results from stellar hydrogen line profiles and the derived lithium abundance. Using an equivalent width upper limit of the strongest Fe I lines (at 3859.91 Å), Keller et al. (2014) determined an upper iron abundance limit of [Fe/H](LTE) < -7.30. Also employing a ⟨3D⟩, NLTE correction for this line from Lind et al. (2012), led to [Fe/H](NLTE) < -7.10. Bessell et al. (2015) redetermined the upper limit in NLTE to [Fe/H](NLTE) $< -7.52 \pm 1\sigma$ using a ⟨3D⟩ model atmosphere and a spectrum with higher signal-to-noise. A microturbulent velocity of 2.0 km s^{-1} was adopted for the star in both studies. More recently, Nordlander et al. (2017) performed a full 3D, NLTE analysis of this star using up-to-date atomic and hydrogen collisional data independent of classical approximations and free parameters. This led to higher iron abundances than Bessell et al. (2015), of [Fe/H](1D, NLTE) < -6.73 and [Fe/H](3D, NLTE) < -6.53, by fitting a stacked spectra in the vicinity of unblended Fe I lines at 3440.6 Å, 3581.2 Å, 3719.9 Å, 3737.1 Å, 3820.4 Å, and 3859.9 Å, respectively. This discrepancy with the Bessell et al. (2015) value was explained as being due to differences in

atomic data and the use of a full 3D model as compared to an averaged ⟨3D⟩ model.

In this work, we adopt an upper limit for $EW_{obs} < 1.0$ mÅ for the strongest Fe I lines at 3608.859 Å and 3859.911 Å, respectively. We find [Fe/H](LTE) < -7.79 using only the resonance line at 3859.911 Å. We also compute [Fe/H](LTE) < -7.24 from the non-resonance line at 3608.859 Å. Our 3859.911 Å result agrees with that of Bessell et al. (2015), [Fe/H](LTE) < -7.80, who used the same line. Our 3608.859 Å LTE value agrees with that of Nordlander et al. (2017) within 0.1 dex (they report [Fe/H](1D, LTE) < -7.34). In NLTE, we determine an upper limit of [Fe/H](NLTE) < -6.52 from the 3608.859 Å line, and [Fe/H](NLTE) < -6.72 from the resonance 3859.911 Å. The abundance obtained from the resonance line is 0.2 dex lower than the 3608.859 Å line. We thus adopt the upper limit of [Fe/H](NLTE) < -6.72 from the resonant line at 3859.911 Å as our final result. This leads to an iron abundance that is 0.80 dex higher than the ⟨3D⟩ NLTE result determined by Bessell et al. (2015; who reported [Fe/H] < -7.52). This result is in perfect agreement with the 1D, NLTE result of Nordlander et al. (2017; who reported [Fe/H] < -6.73). Our 1D NLTE result is, however, 0.19 dex lower than their 3D NLTE value. Overall, Nordlander et al. (2017) report agreement between their 1D and 3D NLTE results, which adds confidence to our result and the use of our NLTE method. As no Fe lines could be detected, we did not compute any NLTE stellar parameters but instead adopt the temperature, gravity, and microturbulent velocity from Bessell et al. (2015).

HE 1327−2326 is a relatively unevolved star located on either the main-sequence or the subgiant branch (Frebel et al. 2005; Aoki et al. 2006; Frebel et al. 2008). Frebel et al. (2005) used color-effective temperature relations from Alonso et al. (1996), to determine $T_{\rm eff} = 6180 \pm 80$ K from broadband *UBVRI* photometry. They used the proper motion to set limits on the distance, and from a 12 Gyr isochrone with [Fe/H] $= -3.5$, two solutions, $\log g = 3.7$ and 4.5, were obtained. Korn et al. (2009) favored a subgiant scenario after carrying out an NLTE Ca I/Ca II ionization equilibrium analysis. The iron abundance of HE 1327−2326 was determined using 10 Fe I lines from Frebel et al. (2008), as no Fe II lines could be detected. For the subgiant case, Frebel et al. (2008) derived [Fe/H](1D, LTE) $= -5.71 \pm 0.2$ and [Fe/H](3D, LTE) $= -6.01 \pm 0.2$. A nominal NLTE correction of 0.2 dex (without any tailored calculation) was adopted in Frebel et al. (2005) following Asplund (2005). A microturbulent velocity of $\xi_t = 1.7$ km s^{-1} was adopted throughout.

We use 10 Fe I lines from Frebel et al. (2008) for our analysis of HE 1327−2326, and additionally a strong Fe II line at 5018.45 Å, for which we use an upper limit of $EW_{obs} < 0.8$ mÅ. Applying our stellar parameter fitting method described in Section 3.1, we find a best fit at $\log g = 3.7$, $T_{\rm eff} = 6130$ K but adopt $\xi_t = 1.7$ km s^{-1}, as in Frebel et al. (2008), given the paucity of lines. These values satisfy both the excitation and ionization equilibrium (to the extent the upper limit allows). We thus also favor the subgiant scenario, in agreement with Korn et al. (2009). Our $T_{\rm eff}$ result agrees well with that of Frebel et al. (2005); however, detecting and measuring any Fe II lines in this star would provide a better constraint on $\log g$. Using our derived stellar parameters, we determine two sets of abundances for each $\log g$ scenario. As such, we derive iron abundances of [Fe/H](LTE) $= -5.82$ and [Fe/H](NLTE) $= -5.16$ for the subgiant case, and [Fe/H](LTE) $= -5.76$ and [Fe/H](NLTE) $= -5.22$ for the dwarf case. Our subgiant LTE Fe abundance agrees with Frebel et al. (2008) within an acceptable 0.11 dex.

HE 0107−5240 is a red giant star (Christlieb et al. 2002). Christlieb et al. (2004) derived $T_{\rm eff} = 5100 \pm 150$ K following $(b - y)$–$T_{\rm eff}$ relations by Alonso et al. (1999, 2001). They used different methods including relative strengths of Balmer line wings and evolutionary tracks to constraint the surface gravity. $\log g = 2.2 \pm 0.3$ dex was eventually adopted. The EWs of 25 Fe I lines were measured and one upper limit of EW < 10 mÅ for the Fe II line at 5018.440 Å. $\xi_t = 2.2 \pm 0.5$ km s^{-1} was determined by forcing the abundances of Fe I lines to have no trend with line strengths. This led to iron abundances of [Fe/H](LTE) $= -5.44 \pm 0.2$. Adopting a nominal NLTE correction of 0.11 dex, they report [Fe/H](NLTE) $= -5.35 \pm 0.2$ (without carrying any detailed NLTE calculation).

Using our EW-fitting method, we determine atmospheric parameters of $T_{\rm eff} = 5050$ K, $\log g = 2.3$, and $\xi_t = 2.2$ km s^{-1}, in good agreement with those presented in Christlieb et al. (2004). Our LTE abundance of [Fe/H](LTE) $= -5.47$ is in very good agreement with that of Christlieb et al. (2004). We then determine [Fe I/H](NLTE) $= -4.72$ and [Fe II/H](NLTE) < -4.71 from the same lines as in Christlieb et al. (2004). We note that the upper limit for the Fe II line (λ5018.44 Å) is already at the level of the Fe I abundance. Should the true Fe II abundance be significantly lower, the surface gravity of the star would need to be significantly increased.

SDSS J1035+0641 is a warm dwarf star (Bonifacio et al. 2015). No metal lines were found in its spectrum except for the Ca II K line and the G-band. Bonifacio et al. (2015) derived $T_{\rm eff} = 6260$ K from a $(g - z)$ calibration, found to be consistent with what was determined from the Hα line wings. Using a 12 Gyr isochrone, two possible values for $\log g$, 4.0 and 4.4, were found. An upper iron abundance limit of [Fe/H](LTE) < -5.59 was set from synthesizing the wavelength region of 3820–3860 Å, where the three strongest Fe I lines are found. Following Caffau et al. (2013), they assumed $\xi_t = 1.5$ km s^{-1} for the microturbulent velocity due to the lack of any Fe lines.

As no iron lines were detected in this star, we could not derive NLTE stellar parameters with our spectroscopic fitting method. Using the $T_{\rm eff}$ and both $\log g$ values, and the 1σ upper limit on the equivalent width for the Fe I line at 3820.425 Å ($EW_{obs} < 5.7$ mÅ) from Bonifacio et al. (2015), we determine identical Fe I upper limit abundances in LTE and NLTE for both cases of $\log g$ of [Fe I/H](LTE) < -5.72 and [Fe I/H](NLTE) < -5.18. The LTE upper limit agrees well with that of Bonifacio et al. (2015) within 0.13 dex.

SDSS J1313−0019 is a star at the base of the red giant branch (Frebel et al. 2015). Its effective temperature $T_{\rm eff} = 5170 \pm 150$ K was determined spectroscopically (LTE) using excitation balance and applying a temperature correction following Frebel et al. (2013). As no Fe II lines could be detected in the spectrum, a surface gravity of $\log g = 2.6 \pm 0.5$ was obtained using a 12 Gyr isochrone at [Fe/H] $= -3.0$. Iteratively, a microturbulent velocity of $\xi_t = 1.8 \pm 0.3$ km s^{-1} and iron abundance of [Fe/H] $= -5.0 \pm 0.1$ were determined.

We determine atmospheric parameters of $T_{\rm eff} = 5100$ K and $\xi_t = 1.8$ km s^{-1}. As no Fe II lines were detected, we could not derive $\log g$ via ionization equilibrium; however, with our

fitting method we obtain a best fit at $\log g = 2.7$. This value could be further investigated with the detection and measurement of Fe II lines. We then used 36 Fe I lines from Frebel et al. (2015) to determine iron abundances of [Fe/H](LTE) = −5.02 ± 0.09 and [Fe/H](NLTE) = −4.41 ± 0.08.

4.2. UMP Stars with −5.0 < [Fe/H] < −4.5

These include SDSS J1029+1729, SDSS J1742+2531, HE 0557−4840, and HE 0233−0343.

SDSS J1029+1729 is a turn-off (TO) star first analyzed by Caffau et al. (2011, 2012). They derived $T_{\rm eff} = 5811 \pm 150$ K from $(g - z)$ color relations from Ludwig et al. (2008) and $\log g = 4.0 \pm 0.5$ from Ca I/Ca II ionization equilibrium (due to the lack of any Fe II lines). They obtained $\xi_t = 1.5$ km s^{-1} following the relation of Edvardsson et al. (1993). Iron abundances were derived as [Fe/H](1D, LTE) = −4.71 ± 0.13 in LTE and [Fe/H](NLTE+3D corr.) = −4.87 ± 0.10, as obtained from adding 3D corrections to a NLTE analysis.

Only 3 Fe I lines could be measured by Caffau et al. (2012). Due to the scarcity of lines, we did not derive any NLTE stellar parameters for this star. Using stellar parameters and the three Fe I EW measurements from Caffau et al. (2012), we derive [Fe/H](LTE) = −4.63 ± 0.13 and [Fe/H](NLTE) = −4.23 ± 0.14. Our LTE value is in agreement with that from Caffau et al. (2012), within error bars.

SDSS J1742+2531 is a warm TO star for which Bonifacio et al. (2015) derived $T_{\rm eff} = 6345$ K, from $(g - z)_0$ colors, and in agreement with that derived from Hα line wings by the authors. Two values for $\log g$ were determined using a 12 Gyr, $Z = 2 \times 10^{-4}$ isochrone: 4.0 for an evolved past TO star case and 4.3 for an unevolved case. $\log g = 4.0$ was eventually adopted, arguing accordance with a metal-poor TO star at this temperature. Using three measured Fe I lines, they derive [Fe/H](LTE) = −4.78 ± 0.08.

We use the same lines to determine [Fe/H](LTE) = −4.82 ± 0.07 and [Fe/H](NLTE) = −4.34 ± 0.03. Due to the scarcity of Fe lines, we refrain from determining other NLTE stellar parameters for this star, and adopt the temperature, gravity, and ξ_t from Bonifacio et al. (2015).

HE 0557−4840 is an evolved red giant star with $T_{\rm eff} = 4900$ K, as determined from fitting Balmer lines (Norris et al. 2007). $\log g = 2.2$ was determined from the Fe I/Fe II and Ca I/Ca II ionization equilibrium, and subsequently $\xi_t = 1.8$ km s^{-1} was obtained. From these stellar parameters they derived [Fe/H](LTE) = −4.80 ± 0.2.

Using 59 Fe I and 1 Fe II lines from Norris et al. (2007), we determine $T_{\rm eff} = 4800$ K, $\log g = 2.4$, and $\xi_t = 1.8$ km s^{-1}. Subsequently, we derive [Fe/H](LTE) = −4.86 and [Fe/H](NLTE) = −4.48, where our LTE value agrees with those of Norris et al. (2013).

HE 0233−0343 is a warm subgiant, and one of three UMP stars first analyzed by Hansen et al. (2014). $T_{\rm eff} = 6100 \pm 100$ K was derived by fitting spectrophotometric observations with 1D, LTE MARCS model atmospheric fluxes and $\log g = 3.4 \pm 0.3$ by employing α-element enhanced, 10 Gyr isochrone at [Fe/H] = −4.7. No Fe II lines were detected in the spectrum. [Fe/H](LTE) = −4.7 ± 0.2 and $\xi_t = 2.0 \pm 0.3$ km s^{-1} were derived from 11 Fe I lines.

Using EW measurements of Fe I lines provided by T. Hansen (2017, private communication), we determine in NLTE $T_{\rm eff} = 6020$ K, $\log g = 3.4$, and $\xi_t = 2.0$ km s^{-1} using the EW-fitting method, and derive [Fe/H](LTE) = −4.44 ± 0.08 and [Fe/H](NLTE) = −3.99 ± 0.06.

4.3. UMP Stars with −4.5<[Fe/H] < −4.0

These include CS 22949−037, SDSS J1204+1201, CD−38 245, HE 1310−0536, HE 2239−5019, SDSS J0140+2344, HE 0057−5959, HE 1424−0241, CS 30336−049, HE 2139 −5432, and SDSS J2209−0028.

CS 22949−037 is a well-studied red giant star (Beers et al. 1992; Depagne et al. 2002; Roederer et al. 2014). Beers et al. (1992) determined [Fe/H](LTE) = −3.80 from a medium-resolution spectrum, using the strength of the Ca II K line. This value was then redetermined by many authors, e.g., Depagne et al. (2002), who derived [Fe/H](LTE) = −3.94, and Roederer et al. (2014), who reported [Fe/H](LTE) = −4.21. Depagne et al. (2002) estimated $T_{\rm eff} = 4900 \pm 125$ K from giant stars' color-calibration relations from Alonso et al. (1999). $\log g = 1.5$ was derived using Fe I/Fe II and Ti I/Ti II ionization equilibrium. Finally, $\xi_t = 1.8$ km s^{-1} was deduced by minimizing the Fe abundance trend as a function of $\log(\mathrm{EW_{obs}}/\lambda)$.

We determine $T_{\rm eff} = 4800$ K, $\log g = 1.9$, and $\xi_t = 1.9$ km s^{-1}, and subsequently derive [Fe/H](LTE) = −3.99 ± 0.16 and [Fe/H](NLTE) = −3.48 ± 0.13 from 65 Fe I and 5 Fe II lines from Depagne et al. (2002). Our LTE result agrees very well with that of Depagne et al. (2002).

SDSS J1204+1201 is an evolved subgiant star (Placco et al. 2015). The authors determined $T_{\rm eff} = 5467 \pm 100$ K from an excitation balance of Fe I lines, $\log g = 3.2 \pm 0.20$ by employing a 12 Gyr isochrone at [Fe/H] = −3.5 and $\xi_t = 1.5 \pm 0.2$ km s^{-1} from Fe I line balances with reduced $\mathrm{EW_{obs}}$. From the above parameters, they derived [Fe/H](LTE) = −4.34 ± 0.05.

We employ our EW-fitting technique to determine $T_{\rm eff} = 5350$ K, $\log g = 3.3$, and $\xi_t = 1.5$ km s^{-1}. [Fe/H](LTE) = −4.39 ± 0.12 and [Fe/H](NLTE) = −3.91 ± 0.11 were then derived using 20 Fe I lines from Placco et al. (2015). No Fe II lines were detected.

CD−38 245 is a red giant star first studied by Bessell & Norris (1984). Cayrel et al. (2004) determined $T_{\rm eff} = 4800 \pm 100$ K following Alonso et al.'s (1999) color-indices calibration, $\log g = 1.5 \pm 0.1$ from Fe I/Fe II and Ti I/Ti II ionization equilibrium and $\xi_t = 2.2 \pm 0.1$ km s^{-1} by minimizing the Fe I abundance-$\mathrm{EW_{obs}}$ trend. Using these stellar parameters, they deduced [Fe/H](LTE) = −4.19.

We determine [Fe/H](LTE) = −4.28 and [Fe/H](NLTE) = −4.03 using 102 Fe I and 7 Fe II lines from Cayrel et al. (2004). Our NLTE stellar parameters are $T_{\rm eff} = 4700$ K, $\log g = 2.0$, and $\xi_t = 2.1$ km s^{1}. While our $T_{\rm eff}$ agrees with that of Cayrel et al. (2004) within error bars, it is worth noting that our $\log g$ value is 0.5 dex higher than theirs.

HE 1310−0536 and HE 2239−5019 are two stars also analyzed by Hansen et al. (2014). Their stellar parameters were derived in the same way as that of HE 0233−0343. The authors derived $T_{\rm eff} = 5000 \pm 100$ K, $\log g = 1.9 \pm 0.3$, [Fe/H](LTE) = −4.2 ± 0.2, and $\xi_t = 2.2 \pm 0.3$ km s^{-1} for HE 1310−0536, and $T_{\rm eff} = 6000 \pm 100$ K, $\log g = 3.5 \pm 0.3$, [Fe/H](LTE) = −4.2 ± 0.2 and $\xi_t = 1.8 \pm 0.3$ km s^{-1} for HE 2239−5019 respectively.

We determine [Fe/H](LTE) = −4.25 ± 0.18 and [Fe/H](NLTE) = −3.77 ± 0.12 from 17 Fe I lines for HE 1310 −0536 and [Fe/H](LTE) = −4.18 ± 0.12 and [Fe/H]

(NLTE) = −3.76 ± 0.09 from 15 Fe I lines for HE 2239 −5019. Our best fit NLTE stellar parameters agree with those derived by Hansen et al. (2014). The Fe I NLTE line abundances are found to have no trend with χ. As no Fe II lines could be detected, we could not test whether the Fe I/Fe II agreement was satisfied. However, future detection and measurements of Fe II lines can better validate our $\log g$ results.

SDSS J0140+2344, CS 30336−049 and HE 2139−5432 are three stars analyzed by Norris et al. (2013). The authors used spectrophotometry, Balmer line-fitting, and Hγ line indices to determine $T_{\rm eff}$ = 5703 ± 60 K, 4725 ± 60 K, and 5416 ± 41 K for SDSS J0140+2344, CS 30336−049, and HE 2139−5432, respectively. For SDSS J0140+2344, no Fe II lines were measured, and the authors employed a 12 Gyr isochrone to determine two $\log g$ values: 4.7 for a dwarf case and 3.4 for a subgiant. Two corresponding values of 0.8 km s^{-1} and 1.5 km s^{-1} for ξ_t and −4.00 and −4.09 for [Fe/H](LTE) were determined, respectively. For CS 30336−049, 3 Fe II lines were detected, and 1 Fe II line was detected for HE 2139 −5432. Using Fe I/Fe II ionization equilibrium, they derived $\log g$ = 1.2 and $\log g$ = 3.0 for CS 30336−049 and HE 2139 −5432, respectively. From these parameters, ξ_t = 2.1 km s^{-1} and [Fe/H](LTE) = −4.03 for CS 30336−049 and ξ_t = 0.8 km s^{-1}, and [Fe/H](LTE) = −4.03 for HE 2139 −5432, were determined.

We employed our fitting parameter technique to determine NLTE stellar parameters for these stars. For SDSS J0140+2344, we find $T_{\rm eff}$ = 5600 K, $\log g$ = 4.6, and ξ_t = 1.0 km s^{-1}. Based upon these results, we favor the dwarf scenario over the subgiant case, since our determined $\log g$ = 4.6 resulted from a much better fit of the computed EW to the EW$_{\rm obs}$ than in the subgiant case. Using 35 Fe I lines from Norris et al. (2013), we subsequently determine [Fe/H](LTE) = −4.09 ± 0.13 and [Fe/H](NLTE) = −3.83 ± 0.08 for SDSS J0140+2344. For CS 30336−049 and HE 2139−5432, we use 74 Fe I and 3 Fe II lines and 32 Fe I and 1 Fe II lines from Norris et al. (2013), respectively, to determine $T_{\rm eff}$ = 4685 K, $\log g$ = 1.4, and ξ_t = 2.1 km s^{-1} and $T_{\rm eff}$ = 5270 K, $\log g$ = 3.2 and ξ_t = 1.0 km s^{-1}, respectively. It follows that we obtain [Fe/H](LTE) = −4.22 ± 0.21 and [Fe/H](NLTE) = −3.91 ± 0.16 for CS 30336−049 and [Fe/H](LTE) = −4.00 ± 0.25 and [Fe/H](NLTE) = −3.52 ± 0.17 for HE 2139−5432.

HE 0057−5959 & HE 1424−0241 are two evolved red giant stars studied by Cohen et al. (2004) and Cohen et al. (2008), respectively. Both studies used color indices to determine $T_{\rm eff}$ = 5257 ± 100 K and $T_{\rm eff}$ = 5195 ± 100 K for HE 0057−5959 and HE 1424−0241, and 12 Gyr isochrones to derive $\log g$ = 2.6 and $\log g$ = 2.5, respectively. Removing abundances versus line strength trends, they obtained ξ_t = 1.5 km s^{-1} and ξ_t = 1.8 km s^{-1}. Using these parameters, they derived [Fe/H](LTE) = −4.08 ± 0.2 and [Fe/H](LTE) = −4.05 ± 0.2 for HE 0057−5959 and HE 1424 −0241, respectively.

For HE 0057−5959, we determine [Fe/H](LTE) = −4.28 ± 0.21 and [Fe/H](NLTE) = −3.83 ± 0.12 from 53 Fe I lines from Cohen et al. (2004; no Fe II lines were detected). With our fitting method, we determine NLTE $T_{\rm eff}$ = 5200 K, $\log g$ = 2.8, and ξ_t = 1.9 km s^{-1}. For HE 1424−0241, we use 39 Fe I and 5 Fe II lines to determine [Fe/H](LTE) = −4.19 ± 0.20 and [Fe/H](NLTE) = −3.73 ± 0.15. The LTE results are in good agreement with Cohen et al. (2004) and Cohen et al. (2008). We obtain $T_{\rm eff}$ = 5140 K, $\log g$ = 2.8, and ξ_t = 2.2 km s^{-1} for this star.

SDSS J2209−0028 is a warm dwarf star (Spite et al. 2013). The authors determined $T_{\rm eff}$ = 6440 K using $(g-z)_0$ color calibrations from Ludwig et al. (2008). They assumed $\log g$ = 4.0, which they found to satisfy the Fe I/Fe II ionization equilibrium. They adopted ξ_t = 1.3 km s^{-1} and determined [Fe/H](LTE) = −4.00.

Using 5 Fe I lines from Spite et al. (2013), we determine [Fe/H](LTE) = −3.97 ± 0.13 and [Fe/H](NLTE) = −3.65 ± 0.10. Due to the scarcity of Fe-detected lines, we do not determine other NLTE stellar parameters, but instead adopt those from Spite et al. (2013).

4.4. Final Fe I and Fe II Abundances

We present our final NLTE Fe I and Fe II abundances (whenever possible) and their standard deviations ($\sigma_{\rm stdv}$) in Table 3, computed with the spectroscopically determined NLTE stellar parameters given in Table 2. For comparison, we also present our corresponding LTE values. Despite the scarcity of Fe I and even greater scarcity of Fe II lines, we find that our four-dimensional $T_{\rm eff}$−$\log g$−[Fe/H]−ξ_t spectroscopic EW-fitting method gives consistent Fe I and Fe II abundances to within 0.1 dex without having to force this agreement. This adds confidence in our iron atomic model and method used, in addition to the NLTE derived stellar parameter. Additionally, we find slightly smaller standard deviations in the NLTE Fe abundances compared to LTE for most stars.

Line abundance dispersion can be due to a number of factors, including uncertainties in oscillator strengths and other atomic data, EW measurements, and model hypotheses (1D/3D, LTE/NLTE, …). In this work we try to address these possible causes using the best available *gf*-values, and include a new approximation of hydrogen inelastic collisions in our NLTE modeling. The scatter is indeed reduced for most stars (See Table 3). A full 3D NLTE analysis would likely decrease the scatter even more, but it is still challenging and computationally expensive to employ. In this context, it is encouraging that for SMSS J0313−6708, the only UMP star for which a full 3D NLTE analysis has been performed, Nordlander et al. (2017) report fairly similar 1D NLTE and 3D NLTE results (within 0.2 dex), whereas much larger differences were obtained between LTE and NLTE models. This highlights that accurate abundances can presently be most efficiently obtained with 1D, NLTE models, such as the present study, whenever reliable atomic data are included. A few other full 3D NLTE calculations, however, should be performed to confirm this conclusion.

4.5. Light Element Enhancement Effects on Final Fe Abundances

While Fe is usually considered a good proxy of the overall metal content of most stars, UMP stars can have large abundance enhancements in light and α-elements such C, N, O, Na, Mg, Si, Ca and Ti relative to iron. These elements can be important electron donors and can thus potentially affect the final Fe derived abundances. The feedback contribution from these elements are customarily treated by using α-enhanced input model atmospheres of [α/Fe] = +0.40 for all stars of [Fe/H] < −1.

Table 2
Derived Stellar Parameters of Ultra-metal-poor Stars with Their Slopes (σ^{slope}, for T_{eff} and ξ_t), Variations (σ^{var}, for $\log g$), and Fitting (σ^{fit}, for T_{eff}, $\log g$ and ξ_t) Uncertainties on Their Values (See Section 4.6 for Detailed Descriptions of Each Uncertainty)

Star	T_{eff} (K)	σ^{slope} (K)	σ^{fit} (K)	$\log g$ (cgs)	σ^{var} (cgs)	σ^{fit} (cgs)	ξ_t (km s^{-1})	σ^{slope} (km s^{-1})	σ^{fit} (km s^{-1})	ΔT_{eff} (K)	$\Delta \log g$ (cgs)	$\Delta \xi_t$ (km s^{-1})	Δ[Fe/H] (dex)
$-4.5 <$ [Fe/H] < -4.0													
SDSS J2209−0028	6440[a]	⋯	⋯	4.0[b]	⋯	⋯	1.3	⋯	⋯	⋯	⋯	⋯	0.32
HE 2139−5432	5270	100	43	3.2	0.30	0.15	1.0	0.2	0.2	−146	0.20	0.2	0.48
CS 30336−049	4685	80	35	1.4	0.30	0.22	2.1	0.2	0.1	−40	0.20	⋯	0.31
HE 1424−0241	5140	60	46	2.8	0.40	0.37	2.2	0.3	0.2	−55	0.30	0.4	0.46
HE 0057−5959	5200	110	68	2.8	0.40	0.40	1.9	0.2	0.3	−57	0.20	0.4	0.45
SDSS J0140+2344	5600	100	77	4.6	0.40	0.40	1.0	0.5	0.2	−103	⋯	⋯	0.26
HE 2239−5019	6000	80	49	3.5	0.40	0.40	1.8	0.2	0.1	⋯	⋯	⋯	0.42
HE 1310−0536	5000	70	43	1.9	0.40	0.40	2.2	2.0	1.0	⋯	⋯	⋯	0.48
CD−38 245	4700	60	38	2.0	0.40	0.21	2.1	0.2	0.1	−100	0.50	−0.1	0.25
SDSS J1204+1201	5350	100	45	3.3	0.40	0.40	1.5	0.2	0.2	−117	0.10	⋯	0.48
CS 22949−037	4800	90	67	1.9	0.30	0.20	1.9	0.2	0.2	−100	0.40	0.1	0.51
$-5.0 <$ [Fe/H] < -4.5													
HE 0233−0343	6020	80	52	3.4	0.40	0.40	1.8	0.3	0.2	−80	⋯	⋯	0.45
HE 0557−4840	4800	80	67	2.4	0.30	0.49	1.8	0.4	0.3	−100	0.20	⋯	0.38
SDSS J1742+2531	6345[c]	⋯	⋯	4.0[d]	⋯	⋯	1.5	⋯	⋯	⋯	⋯	⋯	0.48
SDSS J1029+1729	5811[e]	⋯	⋯	4.0[f]	⋯	⋯	1.5	⋯	⋯	⋯	⋯	⋯	0.40
[Fe/H] < -5.0													
SDSS J1313−0019	5100	80	67	2.7	0.40	0.40	1.8	0.2	0.2	−70	0.10	⋯	0.61
SDSS J1035+0641	6260[c]	⋯	⋯	4.0/4.4[d]	⋯	⋯	1.5	⋯	⋯	⋯	⋯	⋯	0.54
HE 0107−5240	5050	60	43	2.3	0.40	0.40	2.2	0.3	0.3	−50	0.10	⋯	0.75
HE 1327−2326	6130	100	32	3.7	0.40	0.40	1.7	0.4	0.3	−50	⋯	0.4	0.66
SMSS J0313−6708	5125[g]	⋯	⋯	2.3[g]	⋯	⋯	2.0	⋯	⋯	⋯	⋯	⋯	**1.07**

Notes. For stars with not enough Fe lines to derive spectroscopic atmospheric parameters, corresponding literature values were adopted (indicated by the table notes below). Columns 11–13 present the NLTE corrections obtained from the differences between our spectroscopic NLTE stellar parameters and previously derived LTE or photometric values. Column 14 shows the NLTE Fe abundance corrections derived in this work.
[a] From photometry; Spite et al. (2013).
[b] Fixed adopted value; Spite et al. (2013).
[c] From photometry and Hα wing-fitting; Bonifacio et al. (2015).
[d] From a 12 Gyr isochrone; Bonifacio et al. (2015).
[e] From photometry; Caffau et al. (2012).
[f] From the Ca I/Ca II ionization equilibrium; Caffau et al. (2012).
[g] From spectrophotometry and H line profile-fitting; Bessell et al. (2015).

Some of the most metal-poor stars have [C/Fe] values of 3 dex or more, with similar O and N abundances, see Table 6 of Placco et al. 2015 for C and N abundances for this sample of UMP stars. Zhao et al. (2016) showed that α-elements such as Mg, Ti and Ca maintained constant values of ∼0.4 relative to Fe for $-2.6 <$ [Fe/H] < -1.0, but with [Ca/Fe] having tendencies to increase below [Fe/H] $= -2.0$, up to 0.6 dex at [Fe/H] $= -2.6$. Other studies of UMP stars, have shown that this ratio can potentially be higher than the canonical [α/Fe] $= +0.40$. Often it also varies from one α-element to another.

A detailed systematic elemental abundance study of UMP stars is therefore needed to quantify how these light element enhancements might affect the iron abundances as well as the stellar parameters of our sample stars. We therefore tested the effects of potential light element enhancements. We thus arbitrarily increased the input metal abundances of the stellar model atmosphere of each UMP star by +0.50 dex, in addition to the standard [α/Fe] $= +0.40$ enhancement.

We then recomputed the final [Fe/H] NLTE abundances, and along the way recorded any potential changes in the spectroscopically determined stellar parameters. The changes are found to be T_{eff}-independent but $\log g$-dependent. Hence, the abundances from Fe I lines are affected, while those from Fe II are hardly changing. Cooler stars display stronger effects upon increasing the metal enhancement than warmer stars. For one of the coolest stars in our UMP sample, CD−38 245 ($T_{eff} = 4700$ K), a change of +0.50 dex in the input model metal abundance results in a 0.25 dex decrease in the average Fe I abundances and a slight 0.02 dex increase in the Fe II abundances. This corresponds to a compensated −0.20 dex change in $\log g$. For a hotter star, HE 2139−5432 ($T_{eff} = 5270$ K), smaller changes of −0.06 dex were obtained for Fe I and 0.02 dex for Fe II, while negligible differences were noted for the other stellar parameters, including a ξ_t change of −0.02 km s^{-1}. For the even hotter star, J1204+1201 ($T_{eff} = 5350$ K), smaller differences of 0.01 dex for Fe I were obtained.

On average, for most UMP stars within $5000 < T_{eff} <$ 7000 K, this additional metal abundance enhancement of +0.50 dex thus causes a slight decrease in the final Fe abundance by at most ∼0.05 dex. This value is much smaller

Table 3
Our Results for the Average Fe I, Fe II, and Total Fe Abundances with Their Standard Deviation Errors Obtained for the UMP Stars, Both in LTE and NLTE, Respectively

Star	[Fe I/H]^{LTE}	[Fe II/H]^{LTE}	[Fe I/H]^{NLTE}	[Fe II/H]^{NLTE}	[Fe/H]^{LTE}	[Fe/H]^{NLTE}	N Fe I	N Fe II
				$-4.5 <$ [Fe/H] < -4.0				
SDSS J2209−0028	−3.97 ± 0.13	···	−3.65 ± 0.10	···	−3.97 ± 0.13	−3.65 ± 0.10	5	0
HE 2139−5432	−4.01 ± 0.25	−3.53	−3.52 ± 0.17	−3.54	−4.00 ± 0.25	−3.52 ± 0.17	32	1
CS 30336−049	−4.23 ± 0.21	−3.83 ± 0.08	−3.91 ± 0.16	−3.86 ± 0.07	−4.21 ± 0.20	−3.91 ± 0.16	74	3
HE 1424−0241	−4.21 ± 0.20	−3.72 ± 0.20	−3.74 ± 0.11	−3.71 ± 0.15	−4.19 ± 0.20	−3.73 ± 0.15	39	5
HE 0057−5959	−4.28 ± 0.21	···	−3.83 ± 0.12	···	−4.28 ± 0.21	−3.83 ± 0.12	53	0
SDSS J0140+2344	−4.09 ± 0.13	···	−3.83 ± 0.08	···	−4.09 ± 0.13	−3.83 ± 0.08	35	0
HE 2239−5019	−4.18 ± 0.12	···	−3.76 ± 0.09	···	−4.18 ± 0.12	−3.76 ± 0.09	15	0
HE 1310−0536	−4.25 ± 0.18	···	−3.77 ± 0.12	···	−4.25 ± 0.18	−3.77 ± 0.12	17	0
CD−38 245	−4.28 ± 0.20	−4.16 ± 0.12	−4.03 ± 0.14	−4.09 ± 0.12	−4.28 ± 0.20	−4.03 ± 0.12	102	7
SDSS J1204+1201	−4.39 ± 0.12	···	−3.91 ± 0.11	···	−4.39 ± 0.12	−3.91 ± 0.11	20	0
CS 22949−037	−3.99 ± 0.15	−3.56 ± 0.10	−3.44 ± 0.12	−3.50 ± 0.09	−3.99 ± 0.16	−3.48 ± 0.13	65	5
				$-5.0 <$ [Fe/H] < -4.5				
HE 0233−0343	−4.44 ± 0.08	···	−3.99 ± 0.08	···	−4.44 ± 0.08	−3.99 ± 0.08	11	0
HE 0557−4840	−4.86 ± 0.17	−4.70	−4.48 ± 0.13	−4.52	−4.86 ± 0.17	−4.48 ± 0.13	59	1
SDSS J1742+2531	−4.82 ± 0.07	···	−4.34 ± 0.03	···	−4.82 ± 0.07	−4.34 ± 0.03	3	0
SDSS J1029+1729	−4.63 ± 0.13	···	−4.23 ± 0.14	···	−4.63 ± 0.13	−4.23 ± 0.14	3	0
				[Fe/H] < -5.0				
SDSS J1313−0019	−5.02 ± 0.10	···	−4.41 ± 0.09	···	−5.02 ± 0.10	−4.41 ± 0.09	36	0
SDSS J1035+0641	$<-5.72 \pm 1\sigma$	···	$<-5.18 \pm 1\sigma$	···	$<-5.72 \pm 1\sigma$	$<-5.18 \pm 1\sigma$	1[a]	0
HE 0107−5240	−5.47 ± 0.20	<−4.70	−4.72 ± 0.15	<−4.71	−5.47 ± 0.20	−4.72 ± 0.15	25	1[a]
HE 1327−2326	−5.82 ± 0.16	<−5.11	−5.16 ± 0.12	<−5.10	−5.82 ± 0.16	−5.16 ± 0.12	10	1[a]
SMSS J0313−6708	$<-7.79 \pm 3\sigma$	···	$<-6.72 \pm 3\sigma$	···	$<-7.79 \pm 3\sigma$	$<-6.72 \pm 3\sigma$	1[a]	0

Notes. The numbers of Fe I and Fe II lines used in the analysis are shown in the last two columns. Values are reported relative to the solar iron abundance of $\epsilon(\mathrm{Fe})_{\odot} = 7.50$ from Asplund et al. (2009).
[a] No line detection, upper limit only.

than the typical error bars and can be thus considered negligible. For cooler stars below 5000 K, however, the enhancement results in larger decreases in the final Fe I abundances of typically 0.2–0.3 dex. If the metal abundance enhancement was pushed to +1.00 dex, the Fe I abundance would decrease by 0.3–0.4 dex. This decrease in the Fe I abundances is due to electron pumping in the atmospheric model upon enhancing the metal model metallicity, thus increasing the electron collisional rates by decreasing the photon mean free path, and hereby pushing the abundances lower toward LTE. Fe II abundances, always being the dominant species, are much less affected by these changes. We note that the second most iron-poor star, HE 1327−2326, which is also extremely enhanced in C, N, and O relative to Fe, is a warm main-sequence star near the TO and thus likely not affected by such model metallicity enhancement changes. The warm giants J1303−0019 and HE 0107−5240, also with large C, N, and O enhancements, on the other hand, might be affected by this at the 0.3–0.5 dex level.

4.6. Uncertainties in Stellar Parameters

We report random and systematic uncertainties on the $T_{\rm eff}$, $\log g$, [Fe/H], and ξ_t of our stellar parameters in Table 2. Our procedure for obtaining stellar parameters results in multiple uncertainties, which we discuss in this section.

Our initial stellar parameters are obtained with a nonlinear fitting method whose uncertainties arise from the covariance matrix in a $T_{\rm eff}$–$\log g$–[Fe/H]–ξ_t parameter space that reflects how constrained the parameters are by the data (both measured and computed EW). Uncertainties depend on the error estimates of the measured EW, which typically vary from 1–5 mÅ. Unfortunately, the EWs used in this work have been adopted from different reference studies that do not always report EW measurement uncertainties. In those cases, we adopt a nominal value of 2 mÅ for all the lines. This value is typical for low S/N spectra of UMP stars (e.g., Caffau et al. 2012; Bonifacio et al. 2015). The resulting typical fitting uncertainties for all our stars are 50 K in $T_{\rm eff}$, 0.2 dex in $\log g$, and 0.2 km s^{-1} in ξ_t. We note that employing a higher value for a nominal EW measurement uncertainty of 5 mÅ would increase the uncertainties up to 100 K in $T_{\rm eff}$, 0.4 dex in $\log g$, and 0.3 km s^{-1} in ξ_t. It is important to note that the 1σ level fitting uncertainties obtained for $\log g$ are underestimated for stars lacking any Fe II line detections. The $\log g$ values obtained from the fitting method for HE 1327−2326, HE 0107−5240, J1313−0019, HE 0233−2343, J1204+1201, HE 1310−0536, HE 2239−5019, J0140+2344, and HE 0057−5959 are driven solely by Fe I lines and thus their uncertainties from the method do not properly reflect the surface gravity dependence on Fe II lines. We therefore decided to use a constant value of 0.40 dex as a $\log g$-fitting uncertainty for these stars, as an average of the values reported by previous studies for $\log g$ of UMP stars with no Fe II lines (e.g., Frebel et al. 2008; Caffau et al. 2012; Bonifacio et al. 2015; Frebel & Norris 2015). Other random uncertainties arise from the uncertainty of the slopes of Fe line abundances versus χ and $\log(\mathrm{EW}/\lambda)$ when obtaining the final

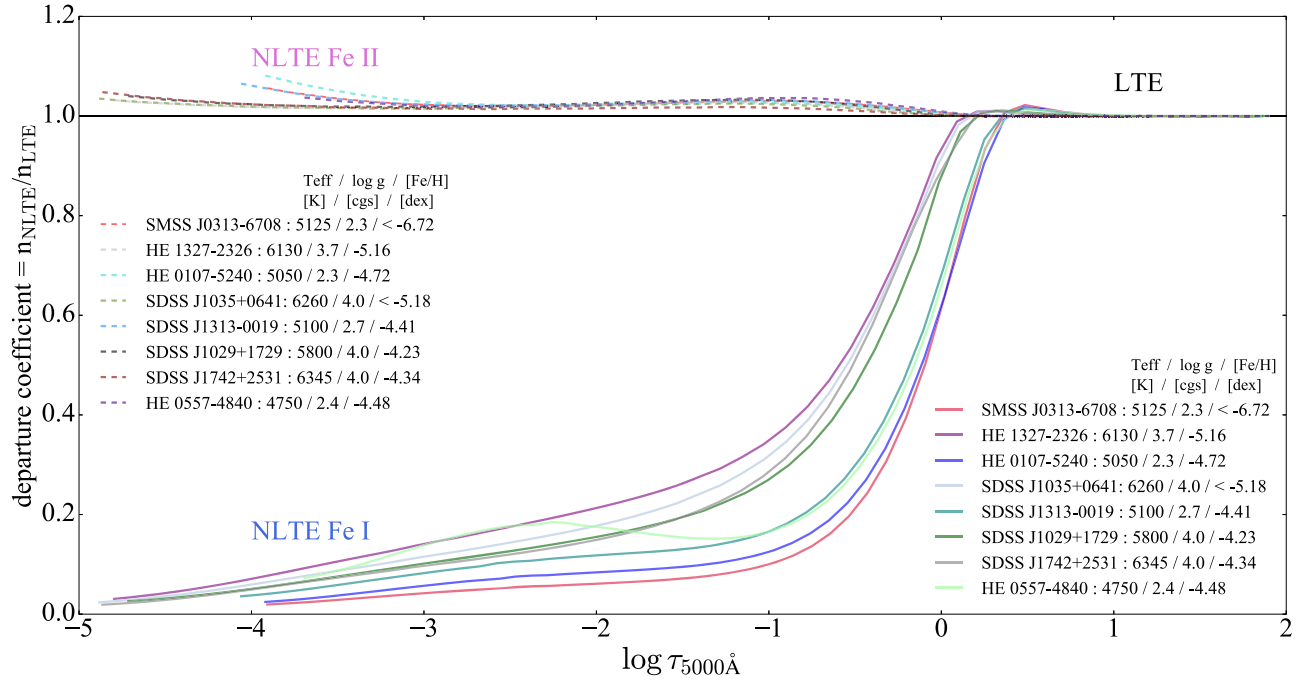

Figure 1. Departure coefficients for eight illustrative UMP stars with [Fe/H] < -4.00. Departures are shown for the ground-level populations of both Fe I and Fe II as a function of optical atmospheric depth τ at 5000 Å. Fe I populations deviate strongly from LTE down to $n_{NLTE}/n_{LTE} \sim 0.1$ at the lowest [Fe/H] for SMSS J0313 −6708, while Fe II population deviations can be considered negligible compared to Fe I.

effective temperature and ξ_t, respectively. Varying the slope within its uncertainty (as determined by the data points) induces a change in the slopes that results in typical uncertainties of 100 K in $T_{\rm eff}$ and 0.2 km s^{-1} in ξ_t. Individual results ($\sigma^{\rm slope}$) for each star are listed in Table 2. Random uncertainties of $\log g$ are determined from varying the ionization equilibrium of Fe I and Fe II within their uncertainties. We adopt the corresponding change as final $\log g$ uncertainty ($\sigma^{\rm var}$), with typical values of 0.3 dex. For stars with no Fe II detection, the same constant value as for the fitting uncertainties of 0.40 dex was used.

We now report uncertainties in our final Fe I and Fe II abundances. First, we report the dispersion in individual line measurements, quantified by the standard deviation ($\sigma^{\rm stdv}$). Typical values are 0.12 dex in NLTE and 0.20 dex in LTE for Fe I. There are not enough Fe II lines to meaningfully quantify this for Fe II, so we adopt the Fe I results instead. We take the standard deviation as our Fe abundance uncertainties because the standard errors of Fe I would be unrealistically small (e.g., 0.02 and less). ($\sigma^{\rm stdv}$) are reported in Table 2. Second, systematic uncertainties arising from varying the stellar parameters $T_{\rm eff}$, $\log g$, and ξ_t by about their uncertainties of ±100 K, ±0.2 cgs, and ±0.2 km s^{-1}, respectively. The resulting changes in the average Fe abundances typically are ±0.07 dex in Fe I and ±0.01 dex for Fe II for changes in $T_{\rm eff}$, ±0.05 dex for Fe I and ±0.2 dex for Fe II for changes in ,log g and finally ±0.1 dex for Fe I and ±0.02 dex for Fe II for changes in ξ_t. Total Fe abundance uncertainties are obtained by summing individual uncertainties ($\sigma^{\rm std}$ and $\sigma^{\rm sys}$) in quadrature. This leads to a typical total average value of 0.13 dex.

Similarly, the total uncertainties in the other stellar parameters are obtained by summing individual uncertainties ($\sigma^{\rm fit}$, $\sigma^{\rm slope}$, and $\sigma^{\rm var}$) in quadrature. This leads to typical total uncertainties of 112 K in $T_{\rm eff}$, 0.45 dex in $\log g$ for stars with Fe II detection, and 0.55 dex for stars without, and 0.4 km s^{-1} in ξ_t. The individual uncertainties for each star are listed in Table 1. These uncertainties reflect the challenge of having available only a limited number of Fe lines in these most iron-poor stars.

5. NLTE Corrections

We now discuss the differences between our NLTE and LTE iron abundances [Fe/H] for the UMP stars. We also report the differences between previously determined stellar parameters ($T_{\rm eff}$, $\log g$, and ξ_t) from the literature (where either full LTE or partial LTE and photometric methods were used). These NLTE corrections for [Fe/H] are shown in Table 3, while those for $\log g$, $T_{\rm eff}$, and ξ_t are listed in Table 1.

5.1. [Fe/H] Abundance Corrections

We define the NLTE Fe line abundance correction for a specific spectral line as the difference between the NLTE and LTE Fe abundance for a given measured equivalent width. We calculate Δ[Fe/H] = [Fe/H]$_{\rm NLTE}$ − [Fe/H]$_{\rm LTE}$, based on the average abundance differences across all individual Fe lines. The results, as well as the number of Fe I and Fe II lines used for each UMP star, are listed in Table 2. The corrections are found to increase with decreasing [Fe/H], which can be understood due to the increasing magnitude of the over-ionization (J_ν–B_ν excess) in the UV. This over-ionization shifts the ionization-recombination balance toward more efficient ionization, thus de-populating the lower levels relative to LTE. This effect grows larger at lower metallicities as radiative rates become more efficient due to the decrease in electron number densities in the optically transparent atmospheric layers (Mashonkina et al. 2011, 2016; Lind et al. 2012). The deviation from LTE in the line formation within the depth of the stellar atmosphere can be seen in Figure 1, where the relative populations (NLTE to LTE) of the ground Fe I level for the UMP stars with [Fe/H] < -4.00 are displayed along their

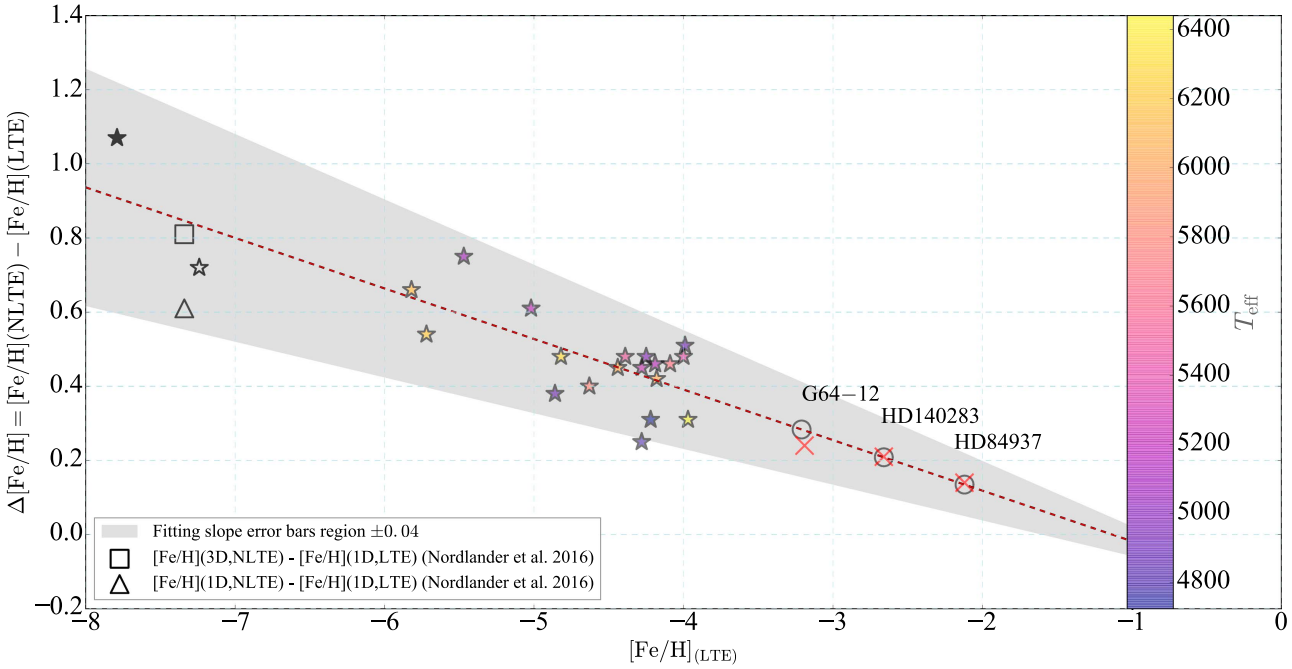

Figure 2. Differences between LTE and NLTE Fe abundances as a function of [Fe/H](LTE). UMP stars are shown as star symbols, and an additional three metal-poor reference stars are shown as open circles. $T_{\rm eff}$ [K] for all stars is color-coded. Black stars, the square, and the triangle represent different possible NLTE corrections obtained for SMSS J0313−6708 as follows: (i) the filled black star is based on using the resonance line at λ3859.911 Å; (ii) the open black star is the correction based on the line at λ3608.859 Å; (iii) the open square is based on 1D NLTE corrections from Nordlander et al. (2017), and (iv) the open triangle is based on the difference between the 3D NLTE and 1D LTE results by Nordlander et al. (2017; see the text for discussion). The red dashed line represents the fit for the UMP stars excluding SMSS J0313−6708. The open circles correspond to NLTE corrections obtained using Equation (1) for the benchmark metal-poor stars HD 140283, HD 84937, and G 64−12. The red crosses correspond to the NLTE corrections obtained by Amarsi et al. (2016). The reference stars agree perfectly with the suggested UMP trend of Δ[Fe/H]. All stars lie within the fitting slope error bar region of ±0.04 (gray shaded region).

atmospheric depths at 5000 Å ($\log \tau_{5000}$). While the departures from LTE increase with decreasing Fe abundances, other factors such as lower gravities and higher effective temperatures can also play a role in the population deviations from LTE throughout the stellar atmospheres (Lind et al. 2012; Mashonkina et al. 2016).

The NLTE corrections as a function of [Fe/H](LTE) for the UMP stars are shown in Figure 2. The data are easily fit with a linear relation:

$$\Delta[\mathrm{Fe/H}] = -0.14\,[\mathrm{Fe/H}]_{\rm LTE} - 0.15. \quad (1)$$

The upper limit correction of Δ[Fe/H] = 1.07 for SMSS J0313−6708 was excluded from the fit as no iron lines detection were made in this star. The fitting fitting slope and Δ[Fe/H]-intercept standard errors are respectively ±0.04 (shown by the gray shaded area in Figure 2) and ±0.18. All the stars, including SMSS J0313−6708, lie within this error bar (gray shaded) region.

This tight relation allows extension of the NLTE corrections to other stars, and potentially also toward higher metallicities ([Fe/H] > −4.00). We test this on the benchmark metal-poor stars HD 84937 ([Fe/H](LTE) = −2.12), HD 140283 ([Fe/H](LTE) = −2.66) and G 64−12 ([Fe/H](LTE) = −3.21) (Amarsi et al. 2016). Using Equation (1), we calculate NLTE corrections of 0.14, 0.22, and 0.29 dex for HD 84937, HD 140283, and G 64−12, respectively. Amarsi et al. (2016) studied these three stars using a full 3D and 1D NLTE analyses, using for the first time quantum mechanical atomic data for hydrogen collisions, and reliable non-spectroscopic atmospheric parameters. The authors report 0.14 dex and 0.21 dex and 0.24 dex as 1D NLTE corrections for HD 84937, HD 140283, and G 64−12, respectively. These values are in excellent agreement with our values. Our fit can thus be used to predict NLTE corrections of metal-poor stars, though the whole range of metallicities [Fe/H] varies from at least −8.00 to −2.00 dex, which further asserts that our relation can be used and applied to LTE Fe abundances of a variety of metal-poor stars.

5.2. *Consequences for Spectroscopic Determination of Stellar Parameters $T_{\rm eff}$ and Log g*

We present in Table 2 the difference in stellar parameters $T_{\rm eff}$, $\log g$, and ξ_t between our NLTE and previously derived LTE spectroscopic or photometric values, whenever possible. This illustrates the changes by going to a full NLTE Fe line analysis. We obtain positive $\Delta \log g = \log g$(NLTE) − $\log g$(lit.value) of 0.1–0.5 dex for all UMP stars whenever a NLTE $\log g$ derivation was possible. An important consequence is that surface gravities derived by LTE analyses tend to be lower than what is expected in NLTE. LTE values should thus be corrected before any further elemental abundance determination. Our positive NLTE $\log g$ corrections are in agreement with previous studies, e.g., Thévenin & Idiart (1999), who have found positive $\Delta \log g$ for a large number of metal-poor stars. Their values were found to be in agreement with spectroscopic independent $\log g$ determinations, e.g., those derived from HIPPARCOS parallaxes.

Our NLTE $T_{\rm eff}$ agree within error bars with the those photometrically derived values using color-$T_{\rm eff}$ calibration relations (e.g., Alonso et al. 1999, 2001). However, comparing values spectroscopically determined through LTE Fe I excitation

equilibrium with our results shows deviations of up to ∼150 K, where NLTE $T_{\rm eff}$ values are lower ($\Delta T_{\rm eff} = T_{\rm eff}({\rm NLTE}) - T_{\rm eff}({\rm lit.value}) < 0$). These deviations can be expected as the LTE Boltzmann equilibrium of atoms cannot pertain at lower metallicities, especially for the non-dominant neutral Fe species, which will affect the excitation balance of Fe I lines.

We treat the microturbulent velocity ξ_t as a free parameter but do not further consider the obtained results for $\Delta\xi_t = \xi_t({\rm NLTE}) - \xi_t({\rm lit.value})$. Nevertheless, we report the obtained values in Table 3.

Given that there is a strong correlation of Δ[Fe/H](LTE) as a function of [Fe/H], we also attempted to determine Δ[Fe/H] as a function of $T_{\rm eff}$ and $\log g$. This requires inspecting lines of similar strengths (EW), and lines with the same lower-level excitation potential χ, as abundances derived from similar lines depend on the thermal stratification of the atmosphere. For example, low-excitation lines are mostly prone to 3D effects that can lower Fe I abundances of metal-poor stars by 0.1 dex (Amarsi et al. 2016). However, due to the small number of UMP stars, and the scarcity of Fe lines, there is not enough data available to map out temperature-dependent and surface-gravity-dependent Δ[Fe/H]. It is thus rather difficult to quantify the dependence of NLTE effects on other parameters than [Fe/H] in our sample of stars. If more stars are found in ongoing and future surveys, this question should be revisited. Nevertheless, spectroscopically derived stellar parameters using the LTE formalism have to be corrected for NLTE effects.

6. Conclusions

We have presented 1D, NLTE Fe line-by-line formation computations for 20 UMP stars with [Fe/H](LTE) $\lesssim -4.0$. We use NLTE Fe I and Fe II lines abundances, when available, to also determine spectroscopic stellar parameters $T_{\rm eff}$, $\log g$ and ξ_t in addition to [Fe/H]. Our results show the following.

1. Our NLTE Fe abundance corrections for the UMP stars are larger than any previous determinations, up to ∼1.00 dex at the lowest iron abundances. These results set a new scale of NLTE corrections to be applied to LTE abundances of other metal-poor stars. The larger corrections are mainly due to performing a full NLTE analysis, using new estimates of hydrogen collision rates and the inclusion of charge-transfer rates for the first time in the NLTE analysis of UMP stars.
2. The line-by-line abundance scatter in NLTE is decreased for most stars down to $\sigma^{\rm stdv} \sim 0.12$ dex as compared to LTE.
3. The NLTE corrections we calculated over the $-7.00 <$ [Fe/H](LTE) < -4.00 range can be extrapolated up to at least [Fe/H] $= -2.00$, to predict NLTE corrections, in perfect agreement with independent (1D and 3D NLTE) determinations.

Even though the number of known UMP stars has greatly increased over the last few years to a sample of 20 stars, the relatively small number remains a shortcoming to a full stellar population analysis. Future surveys are expected to deliver additional UMP stars, hopefully extending to [Fe/H] ~ -7.0. However, now is the time to revisit existing data and to analyze the known stars as precisely and uniformly as possible, as is presented for Fe abundances in this work.

Our results provide a fist step toward a full NLTE chemical species analysis of UMP and EMP stars. A full NLTE abundance pattern will enable us to put constraints on the IMF and other properties of Pop III stars, by comparing accurately computed NLTE abundances of a full set of elements to model supernova yields (e.g., as has been done in LTE by Placco et al. 2015).

We thank the anonymous referee for their useful comments that improved the manuscript. We thank Piercarlo Bonifacio for the useful conversation and advice. We are thankful to Terese Hansen for providing us with equivalent width measurements for some of our studied stars. R.E. acknowledges support from a JINA-CEE fellowship (Joint Institute for Nuclear Astrophysics—Center for the Evolution of the Elements), funded in part by the National Science Foundation under grant No. PHY-1430152 (JINA-CEE). A.F. is supported by NSF-CAREER grant AST-1255160. A.F. acknowledges support from the Silverman Family Career Development Professorship. This work was supported in part by the French-Lebanese Program PHC Cedre. This work has made use of the VALD database, operated at Uppsala University, the Institute of Astronomy RAS in Moscow, and the University of Vienna.

ORCID iDs

Rana Ezzeddine https://orcid.org/0000-0002-8504-8470
Anna Frebel https://orcid.org/0000-0002-2139-7145

References

Abel, T., Bryan, G. L., & Norman, M. L. 2001, in ASP Conf. Ser. 222, The Physics of Galaxy Formation, ed. M. Umemura & H. Susa (San Francisco, CA: ASP), 129
Alonso, A., Arribas, S., & Martinez-Roger, C. 1996, A&A, 313, 873
Alonso, A., Arribas, S., & Martínez-Roger, C. 1999, A&AS, 140, 261
Alonso, A., Arribas, S., & Martínez-Roger, C. 2001, A&A, 376, 1039
Amarsi, A. M., Lind, K., Asplund, M., Barklem, P. S., & Collet, R. 2016, MNRAS, 463, 1518
Aoki, W., Frebel, A., Christlieb, N., et al. 2006, ApJ, 639, 897
Asplund, M. 2005, ARA&A, 43, 481
Asplund, M., Grevesse, N., Sauval, A. J., & Scott, P. 2009, ARA&A, 47, 481
Barklem, P. S., Belyaev, A. K., & Asplund, M. 2003, A&A, 409, L1
Barklem, P. S., Belyaev, A. K., Dickinson, A. S., & Gadéa, F. X. 2010, A&A, 519, A20
Beers, T. C., & Christlieb, N. 2005, ARA&A, 43, 531
Beers, T. C., Preston, G. W., & Shectman, S. A. 1992, AJ, 103, 1987
Belyaev, A. K. 2013, A&A, 560, A60
Belyaev, A. K., & Barklem, P. S. 2003, PhRvA, 68, 062703
Belyaev, A. K., Barklem, P. S., Spielfiedel, A., et al. 2012, PhRvA, 85, 032704
Belyaev, A. K., Yakovleva, S. A., & Barklem, P. S. 2014, A&A, 572, A103
Belyaev, A. K., Yakovleva, S. A., Guitou, M., et al. 2016, A&A, 587, A114
Bergemann, M., Kudritzki, R.-P., Gazak, Z., Davies, B., & Plez, B. 2015, ApJ, 804, 113
Bergemann, M., Lind, K., Collet, R., Magic, Z., & Asplund, M. 2012, MNRAS, 427, 27
Bessell, M. S., Collet, R., Keller, S. C., et al. 2015, ApJL, 806, L16
Bessell, M. S., & Norris, J. 1984, ApJ, 285, 622
Bonifacio, P., Caffau, E., Spite, M., et al. 2015, A&A, 579, A28
Bromm, V. 2013, RPPh, 76, 112901
Bromm, V., Coppi, P. S., & Larson, R. B. 2002, ApJ, 564, 23
Caffau, E., Bonifacio, P., François, P., et al. 2011, Natur, 477, 67
Caffau, E., Bonifacio, P., François, P., et al. 2012, A&A, 542, A51
Caffau, E., Bonifacio, P., François, P., et al. 2013, A&A, 560, A15
Carlsson, M. 1986, UppOR, 33
Carlsson, M. 1992, in ASP Conf. Ser. 26, Cool Stars, Stellar Systems, and the Sun, ed. M. S. Giampapa & J. A. Bookbinder (San Francisco, CA: ASP), 499
Cayrel, R., Depagne, E., Spite, M., et al. 2004, A&A, 416, 1117

Chiaki, G., Yoshida, N., & Kitayama, T. 2012, in AIP Conf. Ser. 1480, First Stars IV- From Hayashi to the Future, ed. M. Umemura & K. Omukai (Melville, NY: AIP), 343
Christlieb, N., Bessell, M. S., Beers, T. C., et al. 2002, Natur, 419, 904
Christlieb, N., Gustafsson, B., Korn, A. J., et al. 2004, ApJ, 603, 708
Cohen, J. G., Christlieb, N., McWilliam, A., et al. 2004, ApJ, 612, 1107
Cohen, J. G., Christlieb, N., McWilliam, A., et al. 2008, ApJ, 672, 320
Collet, R., Asplund, M., & Thévenin, F. 2005, A&A, 442, 643
Depagne, E., Hill, V., Spite, M., et al. 2002, A&A, 390, 187
Drawin, H. W. 1968, ZPhy, 211, 404
Drawin, H. W. 1969a, ZPhy, 225, 470
Drawin, H. W. 1969b, ZPhy, 225, 483
Edvardsson, B., Andersen, J., Gustafsson, B., et al. 1993, A&A, 275, 101
Ezzeddine, R., Merle, T., & Plez, B. 2016a, AN, 337, 850
Ezzeddine, R., Plez, B., Merle, T., Gebran, M., & Thévenin, F. 2016b, arXiv:1612.09302
Frebel, A., Aoki, W., Christlieb, N., et al. 2005, Natur, 434, 871
Frebel, A., Casey, A. R., Jacobson, H. R., & Yu, Q. 2013, ApJ, 769, 57
Frebel, A., Chiti, A., Ji, A. P., Jacobson, H. R., & Placco, V. M. 2015, ApJL, 810, L27
Frebel, A., Collet, R., Eriksson, K., Christlieb, N., & Aoki, W. 2008, ApJ, 684, 588
Frebel, A., Johnson, J. L., & Bromm, V. 2007, MNRAS, 380, L40
Frebel, A., & Norris, J. E. 2015, ARA&A, 53, 631
Gustafsson, B., Bell, R. A., Eriksson, K., & Nordlund, A. 1975, A&A, 42, 407
Gustafsson, B., Edvardsson, B., Eriksson, K., et al. 2008, A&A, 486, 951
Hansen, T., Hansen, C. J., Christlieb, N., et al. 2014, ApJ, 787, 162
Heiter, U., Jofré, P., Gustafsson, B., et al. 2015a, A&A, 582, A49
Heiter, U., Lind, K., Asplund, M., et al. 2015b, PhyS, 90, 054010
Ji, A. P., Frebel, A., & Bromm, V. 2015, MNRAS, 454, 659
Jofré, P., Heiter, U., Soubiran, C., et al. 2014, A&A, 564, A133
Keller, S. C., Bessell, M. S., Frebel, A., et al. 2014, Natur, 506, 463
Klessen, R. S., Glover, S. C. O., & Clark, P. C. 2012, MNRAS, 421, 3217
Korn, A. J., Richard, O., Mashonkina, L., et al. 2009, ApJ, 698, 410
Korn, A. J., Shi, J., & Gehren, T. 2003, A&A, 407, 691
Lambert, D. L. 1993, PhST, 47, 186
Lind, K., Asplund, M., Barklem, P. S., & Belyaev, A. K. 2011, A&A, 528, A103
Lind, K., Bergemann, M., & Asplund, M. 2012, MNRAS, 427, 50
Ludwig, H.-G., Bonifacio, P., Caffau, E., et al. 2008, PhST, 133, 014037
Mashonkina, L., Gehren, T., Shi, J.-R., Korn, A. J., & Grupp, F. 2011, A&A, 528, A87
Mashonkina, L. I., Sitnova, T. N., & Pakhomov, Y. V. 2016, AstL, 42, 606
Nordlander, T., Amarsi, A. M., Lind, K., et al. 2017, A&A, 597, A6
Norris, J. E., Bessell, M. S., Yong, D., et al. 2013, ApJ, 762, 25
Norris, J. E., Christlieb, N., Korn, A. J., et al. 2007, ApJ, 670, 774
Osorio, Y., & Barklem, P. S. 2016, A&A, 586, A120
Osorio, Y., Barklem, P. S., Lind, K., et al. 2015, A&A, 579, A53
Peterson, R. C., & Kurucz, R. L. 2015, ApJS, 216, 1
Placco, V. M., Frebel, A., Lee, Y. S., et al. 2015, ApJ, 809, 136
Plez, B. 2008, PhST, 133, 014003
Roederer, I. U., Preston, G. W., Thompson, I. B., et al. 2014, AJ, 147, 136
Rutten, R. J. 2003, Radiative Transfer in Stellar Atmospheres (Utrecht: Utrecht Univ.)
Scharmer, G. B. 1981, ApJ, 249, 720
Spite, M., Caffau, E., Bonifacio, P., et al. 2013, A&A, 552, A107
Thévenin, F., & Idiart, T. P. 1999, ApJ, 521, 753
Tominaga, N., Iwamoto, N., & Nomoto, K. 2014, ApJ, 785, 98
Wijbenga, J. W., & Zwaan, C. 1972, SoPh, 23, 265
Yakovleva, S. A., Voronov, Y. V., & Belyaev, A. K. 2016, A&A, 593, A27
Zhao, G., Mashonkina, L., Yan, H. L., et al. 2016, ApJ, 833, 225